A highly stable and hierarchical tetrathiafulvalene-based metal-organic framework with improved performance as solid catalyst

Manuel Souto,[a] Andrea Santiago-Portillo,[b] Miguel Palomino,[c] Iñigo J. Vitórica-Yrezábal,[d] Bruno J.C. Vieira,[e] João C. Waerenborgh,[e] Susana Valencia,[c] Sergio Navalón,[b] Fernando Rey,[c] Hermenegildo García,[b,c] Guillermo Mínguez Espallargas*[a]

Herein we report the synthesis of a tetrathiafulvalene (TTF)-based MOF, namely **MUV-2**, which shows a non-interpenetrated hierarchical crystal structure with mesoporous one-dimensional channels of *ca.* 3 nm and orthogonal microporous channels of *ca.* 1 nm. This highly stable MOF (aqueous solution with pH values ranging 2-11 and different organic solvents), possessing the well-known $[Fe_3(\mu_3\text{-}O)(COO)_6]$ secondary building unit, has proven to be an efficient catalyst for the aerobic oxidation of dibenzothiophenes.

Introduction

During the last two decades, the design and preparation of metal-organic frameworks (MOFs)[1–3] have attracted a big deal of attention due to their high potential in several applications such gas storage and separation,[4] sensing,[5] and catalysis,[6] among others. In particular, the combination of both large pores and high stability is of high interest towards practical applications. However, most of reported MOFs are microporous (pore size < 2 nm) and there are only few examples of mesoporous MOFs (2-50 nm) combining both large pores size and high stability such as MIL-100, MIL-101 or PCN-600.[7–9] Recently, the preparation of microporous-mesoporous hierarchical MOFs has become a subject of great interest since micropores contribute to the bulk of the surface area whereas mesopores provide a better accessibility to larger molecules to quickly diffuse, becoming very attractive for catalytic applications.[10] During the last years, several strategies have been reported to construct hierarchical MOFs that usually require multi-step and lengthy synthetic procedures which also lack structural control of the mesopores.[11–14] In contrast, the direct formation of highly-stable and hierarchical MOFs presenting both micro- and mesopores in their crystalline structures (i.e. in an ordered manner) is limited, up to our knowledge, to the material NU-1000, which is based on the $Zr_6(\mu^3\text{-}OH)_8(OH)_8$ cluster and 1,3,6,8-tetrakis(*p*-benzoic acid)pyrene ligand.[15] This material possesses micropores and mesopores that run parallel along the same axis direction. In catalysis, it has been found that the combination of micro- and mesopores in a hierarchical material increases notably its activity by favoring diffusion of substrates and reagents, particularly for bulky reagents.[16]

On the other hand, tetrathiafulvalene (TTF) and its several derivatives are among the most versatile molecules which exhibit interesting redox properties, electron-donor character and potential application as molecular conductors.[17] The use of TTF as a ligand for the design of porous coordination polymers can give rise to multifunctional materials combining different physical properties.[18–20] For example, Dincă and coworkers have recently reported the use of the ligand tetrathiafulvalene tetrabenzoic acid (H_4TTFTB) with various transition metals (II) obtaining a family of isostructural and microporous TTF-based MOFs exhibiting tunable electrical conductivity.[21,22] More recently, the same ligand has also been used for the preparation of a TTF-based MOF with Mg(II) which exhibits permanent mesopores.[23]

Herein, we report the synthesis, structure determination and physical properties of **MUV-2** (MUV: Materials of University of Valencia), a highly stable TTF-based MOF with a unique non-interpenetrated hierarchical crystal structure with mesoporous channels disposed orthogonal to microporous channels. Moreover, the advantages of **MUV-2** respect to widely used MOFs catalyst will be clearly demonstrated for a reaction of large applied interest, illustrating the advantages of having a hierarchical MOF with large mesopores and high stability.

Results and discussion

MUV-2 was prepared according to an adapted synthetic methodology[24] using the preformed cluster $[Fe_3O(CH_3COO)_6]ClO_4$ as starting material. Reaction of $[Fe_3O(CH_3COO)_6]ClO_4$, H_4TTFTB, and acetic acid in *N*,*N*-dimethylformamide (DMF) at 90°C for 72 h yielded dark red needle single crystals of **MUV-2** that were used to determine the crystal structure by single-crystal X-ray diffraction (XRD) (Scheme 1). The bulk material was exhaustively washed with large amount of DMF and immersed in the solvent overnight in order to remove any unreactive starting materials. Finally, the powder was immersed with EtOH at 65°C during 3h, filtered and dried at room temperature. The infrared (IR) spectra of the

nstituto de Ciencia Molecular (ICMol), Universitat de València, c/Catedrático José Beltrán, 2, 46980 Paterna, Spain. E-mail: guillermo.minguez@uv.es
[b.] *Departamento de Química, Universitat Politècnica de València, c/Camino de Vera, s/n, 46022, Valencia, Spain.*
[c.] *Instituto de Tecnología Química (UPV-CSIC), Universitat Politècnica de València-CSIC, Av. De los Naranjos, 46022, Valencia, SPain.*
[d.] *School of Chemistry, University of Manchester, Oxford Road, Manchester, M139PL, United Kingdom*
[e.] *Centro de Ciências e Tecnologias Nucleares, Instituto Superior Téncico, Universidade de Lisboa, 2695-066, Bobadela, LRS, Portugal*
† Supplementary Information (ESI) available. CCDC 1579606 (**MUV-2**).

powder discarded the presence of unreactive starting material (Fig. S1).

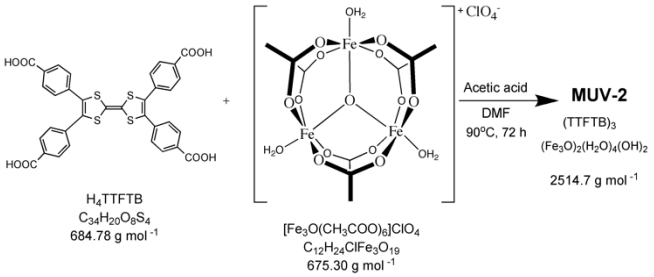

Scheme 1. Synthesis of **MUV-2**.

Single-crystal X-ray diffraction data were collected up to 1 Å resolution at the I19 beamline facilities at Diamond Light Source (UK). **MUV-2** crystallises in the space group *P-62m* and the unit cell parameters are $a = b = 33.3$ Å and $c = 12.4$ Å and consists of 6-connected $[Fe_3(\mu_3\text{-}O)(COO)_6]$ SBUs and tetratopic $TTFTB^{4-}$ ligands. Considering each TTFTB ligand as a four-connected node and each $Fe_3O(COO)_6$ unit as a six-connected node, **MUV-2** can be simplified as a 4,6-connected network with **ttp** topology (Fig. S2), an unusual topology previously observed in two lanthanoid-based MOFs.[25,26] The non-interpenetrated crystal structure reveals large hexagonal mesoporous 1-D channels of *ca.* 3 nm along the *c*-axis which are formed by six TTF ligands and six clusters $[Fe_3(\mu_3\text{-}O)(COO)_6]$ (Fig 1a). TTF moieties are significantly twisted around the central C=C bond with dihedral angle of 20° whereas the planes formed by the two dithiole rings (planes S1-C1-C2-S2 and S3-C5-C6-S4) have a dihedral angle of 41° (Fig. S3). The torsion angles of S2-C3-S1-C1 and C1-C2-S2-C3 are 17° and 11°, respectively, which are typical for neutral TTFs. The phenyl rings exhibit a large distortion respect to the TTF core with dihedral angles of 62° with the latter. In contrast to NU-1000, where microporous channels are running parallel to the mesoporous ones,[15] the crystal structure of **MUV-2** shows that microporous channels of *ca.* 1 nm (9.5 x 12 Å) are disposed orthogonal to the mesoporous channels and are formed between two TTF ligands and two $[Fe_3(\mu_3\text{-}O)(COO)_6]$ clusters (Fig. 1b). In addition, microporous cages are constructed of three TTFTB ligands and two $[Fe_3(\mu_3\text{-}O)(COO)_6]$ SBUs (Fig. 1c) leading to a remarkable open structure with a calculated free volume of *ca*. 82 %. Note that the crystal structure of **MUV-2** contains the precursor $[Fe_3O(CH_3COO)_6]ClO_4$ within the pores since it was determined from the as-synthesised material without the washing and activation procedure.

Mössbauer spectroscopy, magnetic measurements, solid-state cyclic voltammetry and Raman spectroscopy are consistent with the $[Fe_3(\mu_3\text{-}O)(COO)_6]$ cluster being formed by three S = 5/2 Fe(III) ions in octahedral environments, and the TTF ligands being neutral, thus yielding a material with formula $(TTFTB)_3(Fe_3O)_2(H_2O)_4(OH)_2$ which was in agreement with EDAX analysis of **MUV-2** (see Figs. S4-S9). It is important to note that one of the three coordinated H_2O molecules in the cluster is present as negatively charged OH^- hydroxide in order to maintain the charge balance.

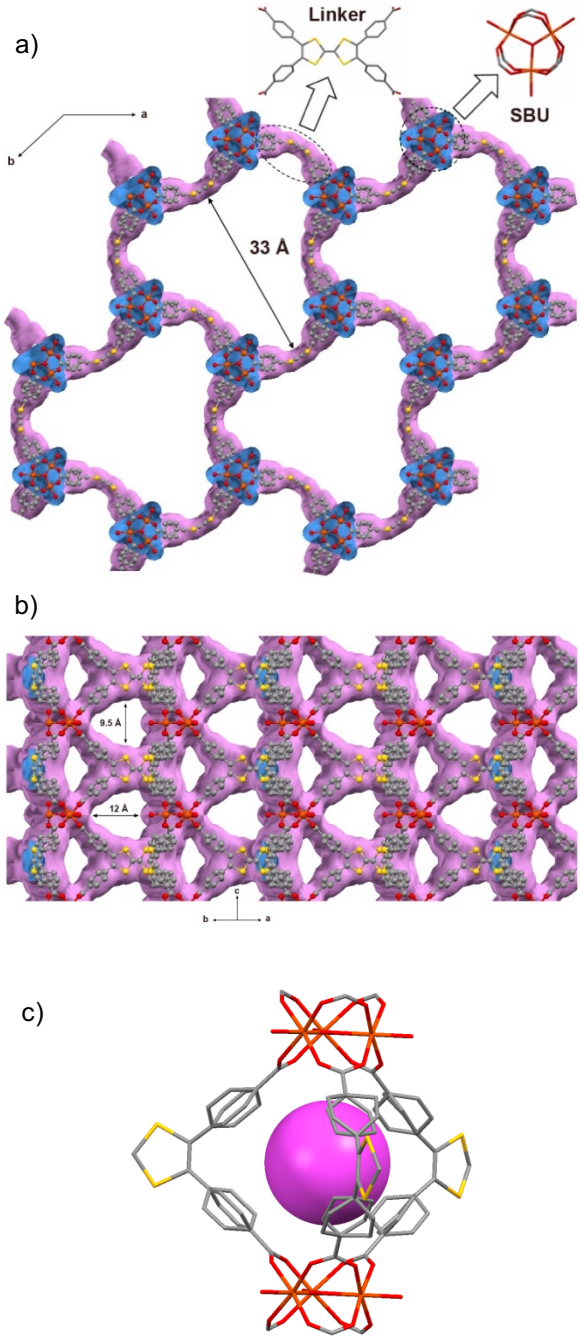

Fig. 1. a) Representation of the crystal structure of **MUV-2** showing mesoporous channels along the *c*-axis and b) microporous channels orthogonal to the *c*-axis. The van der Waals surface is shown in pink. c) Microporous cage formed by three TTFTB ligands and two $[Fe_3(\mu_3\text{-}O)(COO)_6]$ SBUs, with the pink ball placed in the structure to represent the void. The grey, yellow, red and orange ellipsoids represent the C, S, O and Fe atoms, respectively. For simplicity, hydrogens are omitted.

Thermogravimetric analysis (TGA) of washed **MUV-2** exhibited a sharp mass loss of 20 % between 25 and 100 °C which corresponds to the elimination of solvent molecules (Fig. S10). TGA shows a large plateau above 200 °C until the final decomposition at 350 °C.

Activation of **MUV-2** was performed by heating the washed material at 150 °C during 2 h. Its crystallinity was confirmed by powder X-ray diffraction (PXRD) observing that the principal peak is slightly shifted to 3.4° when heating (Fig. 2) and recovers the initial PXRD pattern upon resolvatation (Fig. S11). Additionally, **MUV-2** shows an extraordinary chemical stability in aqueous solutions with pH values ranging from 2-11 and in different organic solvents for 24 h. The PXRD patterns showed that crystallinity is maintained under these conditions (Fig. S12) and the CO_2 adsorption capacity is well preserved, for example, after treatment with pH = 2 and 11 aqueous solution (Fig. S20), with only a minor reduction.

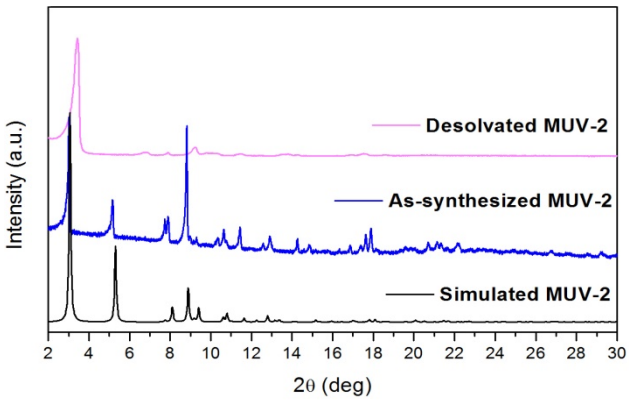

Fig. 2. Powder X-ray diffraction patterns of simulated, as-synthesised and desolvated **MUV-2**.

The N_2 adsorption isotherm at 77 K revealed a combination of Types I and IV isotherms, resulting from the presence of micropores and mesopores, respectively. Thus, a steep N_2 adsorption occurs at low p/p_0 while a slight secondary uptake was also found due to the mesopore filling. It was observed a plateau in the N_2 uptake of 16 mmol/g (Fig. S13). **MUV-2** has a BET surface area of 1220 m^2/g which is higher than those for other reported mesoporous TTF-based MOFs.[23] A micropore volume of 0.52 cm^3/g was found using the Dubinin-Radushkevich equation and the pore size analysis by means of the Barrett-Joyner-Halenda (BJH) method revealed a pore size of 38.7 Å (Fig. S15). Fig. 3 shows the CO_2 and CH_4 isotherms at 298 K, revealing a high sorption capacity for both gases comparable to that of MIL-100.[27]

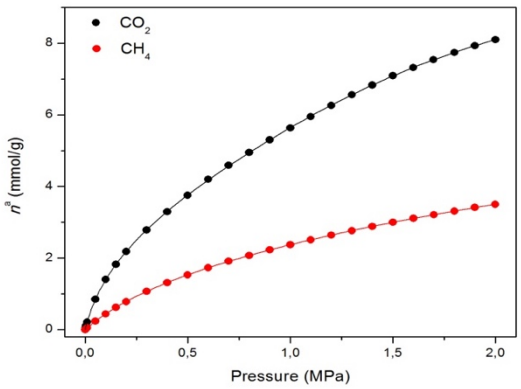

Fig. 3. Gas adsorption isotherms of CO_2 (black) and CH_4 (red) on **MUV-2** at 298 K (lines correspond to the best fits). Data at other temperatures are shown in the Supporting Information.

The isosteric heat of adsorption (q_{st}) of CO_2 decreases from 30 to 20 kJ/mol, which remains constant in the case of CH_4 at around 16 kJ/mol within the studied loading range (Fig. S18). These values clearly indicate the highest affinity of **MUV-2** for the CO_2, rather than for the CH_4. The isosteric heat of adsorption of CO_2 at zero coverage (q_{st}^0) of **MUV-2** is comparable to that of a LTA zeolite of Si/Al ratio of around 6,[28] and that of MIL-101 and in the same range of a wide variety of MOFs.[29]

The superior catalytic activity of **MUV-2** due to the presence of mesopores with respect to widely used MIL MOFs as heterogeneous catalyst was clearly evidenced for the aerobic oxidation of dibenzothiophene (DBT) in long chain alkanes as solvent (Scheme 2). DBT is a model compound of reluctant aromatic sulphur compounds present in diesel.[16] Legal regulations require diminishing the sulphur content in diesel down to the ppb scale. One of the possibilities is to perform oxidation of the fuels to convert the sulphur-containing organic compounds to the corresponding sulfones (generally soluble in water) that can be removed from the fuel by washing. It has recently been reported that DBT can be oxidized by molecular oxygen to the corresponding sulfone ($DBTO_2$) using MIL-101(Cr or Fe) as solid catalyst,[16] although an induction period, probably related to diffusion problems, was observed.

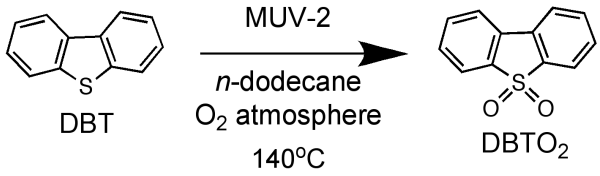

Scheme 2. Aerobic oxidation of DBT to $DBTO_2$ using **MUV-2** as catalyst.

Fig. 4 shows the time conversion plots for DBT disappearance and $DBTO_2$ formation in *n*-dodecane (plotted as sulphur content) comparing the temporal profile using **MUV-2**, MIL-101 (Fe) and MIL-100 (Fe), showing that **MUV-2** is the best performing catalyst. Since all the three MOFs contained the same type of Fe_3-μ_3O active centre, the higher catalytic activity of **MUV-2** can be attributed to the more

favourable diffusion due to the presence of large pores in this material (see Table S3), as demonstrated with three different control experiments. To gain understanding on the origin of the induction period and its dependency on the pore size of **MUV-2**, this solid was contacted with *n*-dodecane containing DBT in the absence of O_2 for 2h, and then O_2 was introduced into the flask, whereby an immediate oxidation of DBT without induction period was observed (see Fig. S21a). A similar observation, i.e. a lack of induction period, was also noted when **MUV-2** was boiled in *n*-dodecane containing O_2 and two hours later DBT was added (see Fig. S21b). Finally, no reduction of the induction period is observed if **MUV-2** is heated in *n*-dodecane for two hours before introducing O_2 and DBT in the system (see Fig. S21c). This rationalisation is in agreement with the fact that, besides higher reaction rates, the induction period is remarkably shortened to about 1 h using **MUV-2**.

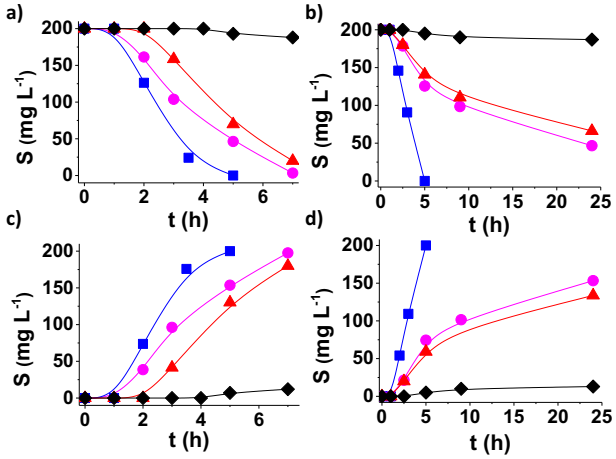

Fig. 4. Aerobic oxidation of DBT (a,b) to $DBTO_2$ (c,d), plotted as sulfur content, using **MUV-2** (■), MIL-101 (Fe) (●), MIL-100 (Fe) (▲) and in the absence of catalyst (♦) using), *n*-dodecane (a, c) or diesel (b, d). Reaction conditions: catalyst: 0.012 mmol of Fe, DBT (1150 mg L^{-1}), solvent (10 mL), O_2 (1 atm), 140 °C.

From the application point of view, desulfuration of diesel should be carried out in the presence of a mixture of hydrocarbons from C13 to C18. Since diffusion is a limiting factor in this condition, the changes from model *n*-dodecane as solvent to real diesel was accompanied by a considerable decrease in activity in the case of MIL-101.[16] It is of interest, therefore, to determine the performance of **MUV-2** for DBT aerobic oxidation in diesel as solvent. The results, presented in Fig. 4b,d, provide a comparison of the time-conversion plots for DBT oxidation using MIL-101(Fe), MIL-100(Fe) and **MUV-2**. As it is observed, the difference in catalytic activity in diesel as solvent remarkably favors **MUV-2**, showing the advantage of this MOF under these conditions. Reusability and productivity tests also show the high stability of **MUV-2** as solid catalyst (Fig. S22 and S23), which is also active for different DBT derivatives (4-MeDBT and 4,6-Me_2DBT) (Fig. S24).

Hot-filtration tests were performed by filtering **MUV-2** out from the hot reaction mixture after 2 h. At this point, the sulphur content was about 125 ppm (cf. the initial 200 mg·L^{-1}), and the clear supernatant was allowed to continue the reaction in the absence of solid particle, observing a very minor progress of about 20 mg·L^{-1} sulphur content decrease in the subsequent 3 h (Fig. S25c). In contrast, a twin reaction in where **MUV-2** was not filtered achieves a complete sulphur removal from initial 200 mg·L^{-1} in 5 h. These results indicate that, after initiation of the reaction, only a very minor contribution of leaching and homogeneous oxidation is occurring. In addition, control experiments using as homogeneous catalysts either chromium (III) acetate (0.6 mg of Cr), the preformed $[Fe_3O(CH_3COO)_6]ClO_4$ at the loadings corresponding to those present in **MUV-2** or leached out during the reaction or H_4TTFTB showed in all cases negligible conversion, indicating that Cr or Fe transition metals at these concentrations or the ligand are not able to promote DBT oxidation (Fig. S25).

A combination of quenching experiments and spectroscopic studies has been used to address the reaction mechanism and, particularly, to determine that the primary reactive oxygen species responsible for oxidation is $HOO^{\cdot}$ (see Fig. S26 and S27). Thus, performing the oxidation in the presence of DMSO, a selective hydroxyl radical scavenger, does not influence much the time-conversion plot, while, in contrast, the presence of *p*-benzoquinone, a selective quencher of superoxide and hydroperoxyl radicals, strongly inhibited DBT oxidation to $DBTO_2$. In addition, admission of oxygen into thermally dehydrated **MUV-2** (220 °C, 5h) at 140 °C leaded to the appearance of two news vibration bands in the Raman spectra at 1502 and 1161 cm^{-1} that can be attributed to physiosorbed and Fe-O-O, respectably (Fig. S27). This metal-peroxo could abstract a hydrogen atom from the medium (*n*-dodecane), generating hydroperoxyl radicals that would initiate DBT oxidation. This hypothesis is supported by the observation of some very minor undetermined oxidation products from *n*-dodecane.

Conclusions

In summary, we have demonstrated that **MUV-2**, which possesses a hierarchical crystal structure with hexagonal mesoporous channels running orthogonal to the micropores, shows high thermal and chemical stability. This hierarchical structure is highly relevant for the catalytic activity of **MUV-2** in the aerobic oxidation of DBT in long chain alkanes as solvents, whereby a dramatic increase in activity with respect to related MIL-100 and MIL-101 has been observed.

Experimental

General methods and materials

All reagents and solvents employed for the syntheses were of high purity grade and were purchased from Sigma-Aldrich Co., and TCI. ^{1}H NMR spectra were recorded using a Bruker DPX300 (300 MHz) spectrometer and Me_4Si as an internal standard. Infrared spectra

were recorded in a FT-IR Nicolet 5700 spectrometer in the 4000-400 cm^{-1} range using powdered samples diluted in KBr pellets. Thermogravimetric analysis was carried out with a Mettler Toledo TGA/SDTA 851 apparatus in the 25-600 ºC temperature range under a 10 ºC/min scan rate and a N_2 flow of 30 $mL \cdot min^{-1}$. Powder X-ray diffraction spectra were recorded using 0.7 mm borosilicate capillaries that were aligned on an Empyrean PANalytical powder diffractometer, using Cu Kα radiation (λ = 1.54056 Å).

Synthesis of MUV-2

Bulk: 20 mg of H_4TTFTB, 20 mg of $[Fe_3O(CH_3COO)_6]ClO_4$ and 0.8 ml of acetic acid were dissolved in 4 ml of DMF in a 10 ml Pyrex vial. The mixture was heated in an oven at 90 °C for 72 h. After cooling down to room temperature, dark brown powder was collected by filtration. The powder was washed with large amount of DMF in order to remove the unreacted ligand and $[Fe_3O(CH_3COO)_6]ClO_4$ and immersed in DMF during one night. Finally, the product was immersed in EtOH during 3 h at 65 °C, washed and collected by filtration (19.6 mg; 80 %).

Crystal data for MUV-2

X-ray data was collected at 100 K on red needles using a synchrotron radiation at single crystal X-ray diffraction beamline I19 in Diamond Light Source, equipped with a Pilatus 2M detector and an Oxford Cryosystems nitrogen flow gas system. Despite of using synchrotron radiation, crystals of **MUV-2** only diffracted to 1.2 Å of resolution. Refinement details can be found in the Supporting Material. Space group *P*-62*m*, *a* = *b* = 33.298(3) Å, *c* = 12.3958(7) Å, *V* = 11903(2) $Å^3$, R_1 (F)= 0.0324, w*R2* (F^2) = 0.0929.

Gas sorption

High-pressure adsorption isotherms of CO_2, CH_4 and N_2 were measured at different temperatures ranging from 283 to 333 K in an IGA-3 gravimetric analyser (Hiden Isochema) using approximately 50 mg of sample placed in the balance. Before each adsorption experiment, the sample was outgassed at 423 K under a final pressure of 10^{-5} Pa for four hours. The sample was then cooled down under high vacuum up to the target temperature that was controlled using a recirculating thermostatic bath. Adsorption measurements were performed by introducing the gas to build up the desired pressures of the isotherms. The heat of adsorption was calculated according to the Clausius–Clapeyron equation from the isotherms measured at different temperatures.

Magnetic measurements

Magnetic susceptibility measurements were carried out on single-phased polycrystalline samples with a Quantum Design MPMS-XL-5 SQUID susceptometer. The susceptibility data were all collected at 1 K min^{-1}, in the range 2-300 K with and applied field of 0.1 T. The susceptibility data were corrected from the diamagnetic contributions as deduced by using Pascal's constant tables.

Mössbauer

Mössbauer spectra were collected in the temperature range 295–4 K in transmission mode using a conventional constant-acceleration spectrometer and a 25 mCi ^{57}Co source in a Rh matrix. The velocity scale was calibrated using α-Fe foil. Isomer shifts, IS, are given relative to this standard at room temperature. The absorber was obtained by packing the powdered samples into a Perspex holder. The absorber thickness was calculated on the basis of the corresponding electronic mass-absorption coefficients for the 14.4 keV radiation. The low temperature spectra were collected in a bath cryostat with the sample immersed in liquid He at 4 K or in He exchange gas at 50 K. The spectra were fitted to Lorentzian lines using a non-linear least-squares method.

Electrochemical measurements

The electrochemical experiments were performed using an Autolab electrochemical workstation (Autolab-128N potentiostat/galvanostat) connected to a personal computer that uses Nova 2.1 electrochemical software. The powdered materials were mixed with Polytetrafluoroethylene (PTFE) in a mass ratio of 90:10 in ethanol and deposited on a 3 mm glassy carbon disc working electrode (which was polished sequentially with 0.3, 0.1 and 0.05 μm alumina powders and washed with deionised water before each experiment). A typical three-electrode experimental cell equipped with a platinum wire as the counter electrode, and a silver wire as the pseudoreference electrode was used for the electrochemical characterization of the working electrodes. All measurements were carried out with magnetic agitation and nitrogen bubbling. The electrochemical properties were studied measuring the CV at different scan rates in 0.1 M $TBAPF_6/CH_3CN$ solution. Ferrocene was added as an internal standard upon completion of each experiment. All potentials are reported in V versus Ag/AgCl.

Catalytic experiments

5 mg of catalyst was placed on a round-bottom flask (25 mL). Activation of the **MUV-2** catalyst was carried out by heating at 150 °C under vacuum overnight. Subsequently, the reaction temperature was fixed at 140 °C and the required reaction atmosphere was obtained by purging the system with a balloon containing O_2 under atmospheric pressure. The reaction time started by addition of a solution of DBT (200 mg L^{-1} of S) in 10 mL of the reaction solvent to the preheated round-bottom flask. As reaction solvent, *n*-dodecane or commercial diesel (Repsol) were used. The mixture was continuously stirred magnetically at 500 rpm. The course of the reaction was followed by sampling 250 μl of the reaction mixture that was diluted with 250 μl of anisole and injected in a GC having a FI detector and a 30 m capillary column of 5% crosslinked phenyl methyl silicone. At the end of the reaction, the mixture was filtered to remove the solid while still hot and the organic phase was washed with three aliquots of 20 ml of water to remove the $DBTO_2$ product

formed in the process. Selective radical quenching experiments using *p*-benzoquinone or DMSO were carried out as described above but with the addition of 20 mol% of these reagents with respect to the initial DBT at 1.5 h of the reaction time.

Conflicts of interest

There are no conflicts to declare.

Acknowledgements

The work has been supported by the European Union (ERC-2016-CoG 724681-S-CAGE) and from the Spanish MINECO (CTQ 2014-59209-P). We also thank the Spanish government for the provision of a Severo Ochoa project (SEV-2012-0267) and a María de Maeztu project (MDM-2015-0538). G.M.E. thanks MINECO for a Ramón y Cajal fellowship. We thank J. M. Martínez-Agudo, G. Agustí and J. Romero from the University of Valencia for magnetic and cyclic voltammetry measurements. We thank the Diamond Light Source (UK) for synchrotron beamtime. C^2TN/IST authors acknowledge the Portuguese Foundation for Science and Technology (FCT), contract UID/Multi/04349/2013.

Author Contributions

M. S. synthesised and characterised the material; G. M. E. and I. J. V.-Y. contributed to solution and refinement of the structure from single crystal data; A. S.-P., S. N. and H. G. carried out and analysed the catalytic experiments; B. J. C. V. and J. C. W. carried out and analysed the Mössbauer measurements; M. P., S. V. and F. R. carried out measurements and analysis of adsorption isotherms; M. S. and G. M. E. conceived the research and prepared the manuscript; all authors made comments on the manuscript.

References

1 H. Furukawa, K. E. Cordova, M. O'Keeffe and O. M. Yaghi, *Science*, 2013, **341**, 1230444.

2 H.-C. Zhou and S. Kitagawa, *Chem. Soc. Rev.*, 2014, **43**, 5415–5418.

3 G. Maurin, C. Serre, A. Cooper and G. Férey, *Chem. Soc. Rev.*, 2017, **46**, 3104–3107.

4 K. Sumida, D. L. Rogow, J. A. Mason, T. M. McDonald, E. D. Bloch, Z. R. Herm, T. H. Bae and J. R. Long, *Chem. Rev.*, 2012, **112**, 724–781.

5 G. Mínguez Espallargas and E. Coronado, *Chem. Soc. Rev.*, 2018, doi: 10.1039/c7cs00653e.

6 S. M. J. Rogge, A. Bavykina, J. Hajek, H. Garcia, A. I. Olivos-Suarez, A. Sepúlveda-Escribano, A. Vimont, G. Clet, P. Bazin, F. Kapteijn, M. Daturi, E. V. Ramos-Fernandez, F. X. Llabrés i Xamena, V. Van Speybroeck and J. Gascon, *Chem. Soc. Rev.*, 2017, **46**, 3134–3184.

7 G. Férey, C. Mellot-Draznieks, C. Serre, F. Millange, J. Dutour, S. Surblé and I. Margiolaki, *Science*, 2005, **309**, 2040–2042.

8 P. Horcajada, S. Surble, C. Serre, D.-Y. Hong, Y.-K. Seo, J.-S. Chang, J.-M. Greneche, I. Margiolaki and G. Ferey, *Chem. Commun.*, 2007, **100**, 2820–2822.

9 K. Wang, D. Feng, T. F. Liu, J. Su, S. Yuan, Y. P. Chen, M. Bosch, X. Zou and H. C. Zhou, *J. Am. Chem. Soc.*, 2014, **136**, 13983–13986.

10 Y. Yue, P. F. Fulvio and S. Dai, *Acc. Chem. Res.*, 2015, **48**, 3044–3052.

11 L. Li, S. Xiang, S. Cao, J. Zhang, G. Ouyang, L. Chen and C.-Y. Su, *Nat. Commun.*, 2013, **4**, 1774.

12 G. Cai and H. L. Jiang, *Angew. Chem. Int. Ed.*, 2017, **56**, 563–567.

13 B. Bueken, N. Van Velthoven, T. Willhammar, T. Stassin, I. Stassen, D. A. Keen, G. V. Baron, J. F. M. Denayer, R. Ameloot, S. Bals, D. De Vos and T. D. Bennett, *Chem. Sci.*, 2017, **8**, 3939–3948.

14 J. Koo, I.-C. Hwang, X. Yu, S. Saha, Y. Kim and K. Kim, *Chem. Sci.*, 2017, **0**, 1–5.

15 J. E. Mondloch, W. Bury, D. Fairen-Jimenez, S. Kwon, E. J. Demarco, M. H. Weston, A. A. Sarjeant, S. T. Nguyen, P. C. Stair, R. Q. Snurr, O. K. Farha and J. T. Hupp, *J. Am. Chem. Soc.*, 2013, **135**, 10294–10297.

16 A. Gómez-Paricio, A. Santiago-Portillo, S. Navalón, P. Concepción, M. Alvaro and H. Garcia, *Green Chem.*, 2016, **18**, 508–515.

17 N. Martín, *Chem. Commun.*, 2013, **49**, 7025–7.

18 H.-Y. Wang, L. Cui, J.-Z. Xie, C. F. Leong, D. M. D'Alessandro and J.-L. Zuo, *Coord. Chem. Rev.*, 2017, **345**, 342–361.

19 H.-Y. Wang, J.-Y. Ge, C. Hua, C.-Q. Jiao, Y. Wu, C. F. Leong, D. M. D'Alessandro, T. Liu and J.-L. Zuo, *Angew. Chem. Int. Ed.*, 2017, **56**, 5465 –5470.

20 L. Sun, M. G. Campbell and M. Dincă, *Angew. Chem. Int. Ed.*, 2016, **55**, 3566–3579.

21 T. C. Narayan, T. Miyakai, S. Seki and M. Dincă, *J. Am. Chem. Soc.,* **134**, 2012, 12932–12935.

22 S. S. Park, E. R. Hontz, L. Sun, C. H. Hendon, A. Walsh, T. Van Voorhis and M. Dincă, *J. Am. Chem. Soc.*, 2015, **137**, 1774–1777.

23 S. S. Park, C. H. Hendon, A. J. Fielding, A. Walsh, M. O'Keeffe and M. Dincă, *J. Am. Chem. Soc.*, 2017, **139**, 3619–362276.

24 D. Feng, K. Wang, Z. Wei, Y.-P. Chen, C. M. Simon, R. K. Arvapally, R. L. Martin, M. Bosch, T.-F. Liu, S. Fordham, D. Yuan, M. a Omary, M. Haranczyk, B. Smit and H.-C. Zhou, *Nat. Commun.*, 2014, **5**, 5723.

25 Structure with RefCode QUVDEO also has **ttp** topology. K. Liu, H. Li, X. Zhang, W. Shi and P. Cheng, *Inorg. Chem.*, 2015, **54**, 10224−10231.

26 Structure with RefCode XIFHIF also has **ttp** topology. H. Li, W. Shi, K. Zhao, Z. Niu, H. Li and P. Cheng, *Chem. Eur. J.*, 2013, **19**, 3358–3365.

27 P. L. Llewellyn, S. Bourrelly, C. Serre, A. Vimont, M. Daturi, L. Hamon, G. De Weireld, J. Chang, D. Hong, Y. K. Hwang and S. H. Jhung, *Langmuir*, 2008, 7245–7250.

28 M. Palomino, A. Corma, F. Rey and S. Valencia, *Langmuir*, 2010, **26**, 1910–1917.

29 S. Xiang, Y. He, Z. Zhang, H. Wu, W. Zhou, R. Krishna and B. Chen, *Nat. Commun.*, 2012, **3**, 954.